Journal of Materials Chemistry A

PAPER

View Article Online
View Journal | View Issue

Cite this: J. Mater. Chem. A, 2016, 4, 6989

Nature inspiring processing route toward high throughput production of perovskite photovoltaics†

Hidetaka Ishihara,‡[a] Som Sarang,‡[b] Yen-Chang Chen,‡[a] Oliver Lin,[ac] Pisrut Phummirat,[a] Lai Thung,[a] Jose Hernandez,[a] Sayantani Ghosh[b] and Vincent Tung*[ac]

We report our results of developing perovskite thin films with high coverage, improved uniformity and preserved crystalline continuity in a single pass deposition. This approach, inspired by the natural phenomena of tears of wine, works by regulating the hydrodynamics of the material comprising of droplets during spray-pyrolysis. In contrast to conventional spray-pyrolysis where droplets dry independently and form a rough morphology, the use of binary solvent system creates localized surface tension gradients that initiate Marangoni flows, thus directing the incoming droplets to spontaneously undergo coalescing, merging and spreading into a continuous wet films before drying. By systematically exploring the dynamics of spreading and drying, we achieve spray-coated perovskite photovoltaics with power conversion efficiency of 14.2%, a near two-fold improvement than that of the spray-pyrolysis counterpart. Of particular significance is the fact that the single pass deposition technique unveils novel inroads in efficient management of lead consumption during deposition.

Received 7th December 2015
Accepted 18th February 2016

DOI: 10.1039/c5ta09992g

www.rsc.org/MaterialsA

[a]School of Engineering, University of California, Merced, California 95343, USA. E-mail: vtung@lbl.gov
[b]School of Natural Science, University of California, Merced, California 95343, USA
[c]Molecular Foundry, Lawrence Berkeley National Lab, Berkeley, California 94720, USA

† Electronic supplementary information (ESI) available. See DOI: 10.1039/c5ta09992g

‡ These authors contributed equally to this work.

Sayantani Ghosh is an Associate Professor of Physics at the University of California, Merced. She received her PhD in Physics at the University of Chicago in 2003, and was a SUN microsystems postdoctoral fellow at the University of California, Santa Barbara till 2006. Her group's research interests span traditional topics in condensed matter along with emerging multi-disciplinary themes, focusing on the physics of novel materials and developing techniques and protocols to manipulate their properties for applications in energy storage and information processing devices. She is the recipient of a NSF CAREER award.

Vincent Tung is an Assistant Professor at the School of Engineering, University of California, Merced and affiliated with the Molecular Foundry, Lawrence Berkeley National lab. He received his Ph.D. degree in materials science and chemistry from the University of California, Los Angeles in 2009 and became an Initiative for Sustainability and Energy at Northwestern (ISEN) postdoctoral research fellow at the Northwestern University in 2010. His main research interest is in the general area of material chemistry and assembly for energy harvesting and storage. He is the recipient of an America Chemical Society Petroleum Fund New Doctoral Investigator Award, and the Research Excellence Early Career Investigator Award by the Graduate Council at the University of California. He is also a die-hard fan of Red Sox and enjoys a cup of coffee at Blue Bottle and Sight glass.

1. Introduction

Nature provides a vast range of inspiring examples of diverse and complex nanostructures in order to achieve several essential functions. For example, the hydrophobic surface on a lotus leaf allows it to self-clean from its residing environment. The microstructure of cork reveals how biological cellular materials can be lightweight yet mechanically resilient, an efficient assembly that allows individual cells to form a honeycomb arrangement. Another compelling example is the formation of "tears of wine". Upon a quick agitation, an instantaneous construction of uniform, self-organizing liquid thin film can be created on virtually any hard surfaces regardless of texture, surface chemistry, and curvatures. In addition, the dissimilar evaporation characteristics of individual solvents drive the initially stationary solvent fronts towards un-wetted area, thus leading to a nearly full coverage of uniform thin films. Specifically, such a scalable, and facile process that allows reproducible control of thickness, and morphological homogeneity at the nanoscale holds tantalizing prospect for printable solar cells, particularly the emerging inorganic–organic perovskite (PVSK) photovoltaics.

Rapid advancement in PVSKs has spurred immense interests because of their high absorption coefficient,[1] low processing temperature,[2–4] high charge carrier lifetime,[5] appropriate bandgap, and exceptional charge transport dynamics,[6,7] thus giving rise to the grid-competitive power conversion efficiency (PCE, >20%).[2,3,8–10] While the prospect of harnessing these advantageous properties makes PVSKs ideal candidates for next generation solar cells, there are roadblocks hindering widespread deployment. Two of the major challenges are: (a) the lack of a scalable processing route that enables rapid deposition of uniform thin films with both the material quality and morphology, and (b) perplexingly high lead (Pb) consumption during processing. To address these challenges, extensive research has been carried out in the following directions: large area coating of PVSKs with crystalline domains exceeding micrometers is made possible by the doctor blading. Meanwhile, manipulation of de-wetting process has shown to induce the growth of PVSK crystals with high aspect ratio domains. Hot casting of PVSK precursors results in the unique lotus leaf like patterns with lateral dimensions surpassing millimeter scale.[11] While strenuous efforts in these areas have shed light on the aforementioned challenges, the need for additional processing steps to improve the morphology as well as the crystallinity adversely interrupts the fabrication process and creates extra manufacturing complication as well as cost when scaling up.[4,9,12–19] Further, excessive amounts of PVSK precursor solutions are typically a prerequisite to ensure the uniform coverage, thus generating unwanted Pb wastes. Alternatively, spray-pyrolysis, where fine droplets are driven towards the substrates through continuous flow of gas media has been suggested to address the prior challenges.[20] Spray-pyrolysis is performed at atmospheric pressure using low cost equipment with a roll-to-roll process capability. To constitute the thin film, precursor-containing droplets are continuously deposited in a multi-pass manner until a desired thickness and coverage are achieved. Specifically, the amount of solute directly scales with volume of precursor solutions deposited on the substrates, effectively reducing the consumption of Pb during deposition. Unfortunately, microscopic characterizations have revealed that the as-fabricated thin film comprises discrete crystals randomly stacked in both in-plane and out-of-plane directions, which is due to complex droplet hydrodynamics.

The mechanism of thin film formation enabled by spray-pyrolysis can be essentially divided into three stages, which are (i) droplet deposition, (ii) de-wetting and (iii) annealing. Upon deposition, droplets may undergo either coalescing, spreading or receding. In the case of spray-pyrolysis, droplets typically impinge on a hot surface and thus receding dominates. As a result, these droplets immediately pin on to the substrate; thereby forming stationary contact lines. Next, de-wetting process drives the rupture of wet films to minimize the total surface energy, leading to the formation of radial, discontinuous patterns, *i.e.* coffee-ring effect.[21,22] However, droplets may impinge on a thin film of liquid or wet lamellae already formed on the substrate as a result of the impaction of the earlier droplets because of the multi-pass deposition. In other words, wet films or drying patterns are continuously bombarded during the course of deposition, therefore creating rough, crater-like morphology.[20] Finally, annealing process converts the textured PVSK precursors into crystallized films. It is known that the carrier transport within PVSK greatly hinges on the homogeneity, integrity and continuity of crystalline networks. As a result, the transport pathways that comprise high densities of intra- and inter-granular defects collectively limit the efficient harvesting of photo-dissociated charge carriers at the collecting electrodes, thus plummeting the overall PCE.[23,24]

In this light, a single-pass deposition that can preferentially regulate the hydrodynamics of incoming droplets should greatly improve the morphology, and homogeneity of the thin films while reducing the reliance on environmentally toxic Pb through an efficient management during deposition. In this work, we demonstrate that PVSK thin films with a nearly complete coverage, improved morphology and preserved crystalline continuity can be readily and rapidly created by "tears of wine" inspired electrohydrodynamic (EHD) nano-manufacturing route. Instead of the unwanted de-wetting and bombarding processes, PVSK containing droplets directly coalesce with neighboring droplets upon deposition, followed by spreading and ultimately merging into uniform thin films. The resulting PVSK photovoltaics with a planar architecture already deliver improved PCE of averaging 14% with high reproducibility.

2. Experimental section

Preparation of PVSK precursor solutions

Hydroiodic acid (HI) (57 wt% in water), methylamine (CH_3NH_2) (2 M in methanol), DMF (anhydrous, 99.8%), NMP (anhydrous, 99.5%), DMSO (anhydrous 99.7%), dichlorobenzene (anhydrous, 99%), diethyl ether (anhydrous, 99%) and $PbCl_2$ (99.999%) were used as received from Sigma Aldrich.

Methylammonium iodide (CH_3NH_3I, MAI) was synthesized through a modified strategy by reacting 4.2 mL of HI with 15.8 mL of CH_3NH_2 at 0 °C for 2 hours in a three-neck flask under a nitrogen atmosphere with constant stirring. The solvent was evaporated from the mixture using a rotary evaporator and a MAI white precipitation was collected. The crude product was washed with diethyl ether three times and dried under vacuum at 60 °C overnight. The dried powder was stored inside a glove box. 420 mg mL^{-1} of MAI and 245 mg mL^{-1} of $PbCl_2$ were mixed together in a mixture of DMSO and NMP (4 : 6, v/v) at 60 °C for 12 h until no visibly distinguishable precipitation. The final concentrations of MAI and $PbCl_2$ are 2.64 M and 0.88 M, respectively.

Marangoni-assisted deposition of PVSK

The PVSK precursor solutions with various solvent combinations and volume ratios were fed through a programmable syringe pump at the constant feeding rate of 18 μL min^{-1}. A high DC voltage (12.5 kV) is applied between the spinneret and the substrate holder. The distance between the nozzle tip and the ground was kept at 2.5 cm. A multi-jet mode is employed throughout the deposition due to the high coverage and uniformity of droplets. A thermal couple was mounted on to a computer controlled moving stage to closely monitor the surface temperature. The moving speed of the linear motor stage (Newport, ILS 100LM) was programmed at 3.2 mm s^{-1} for the single-pass deposition. The total deposition time is 6 to 8 seconds for the thin film thickness of 600 nm. Note that we suggest controlling the speed of moving stage as opposed to altering the concentrations of PVSK precursors for achieving various thicknesses. Finally, the whole EHD was carried out in a humidity controlled (<15%) fume hood and monitored by a high-speed camera (Phantom) in order to visualize the droplet dynamics.

Device fabrication

Indium tin oxide (ITO) substrates were treated with UV/ozone for 20 minutes, followed by depositing PEDOT:PSS (AI 4083, Clevios) as the hole transport layer. After spin-coating, the thin film was annealed at 120 °C for 20 min. Prior to EHD deposition of PVSK precursors, additional UV/ozone treatment (40 seconds) was employed to enhance the hydrophilicity as well as removing any remaining organic contaminants. The substrate temperature was kept at 35 °C to avoid the unwanted coffee ring effect. Flow rate was set at 18 μL min^{-1} while the moving speed of the linear motor stage was programmed at 3.2 mm s^{-1}. Note that humidity of the fume hood is closely monitored to keep at below 15%. The resulting substrates are immediately transferred to a glass Petri dish for 15 minutes to facilitate the Marangoni flow driven dynamic growth of PVSK grains. On the other hand, to emulate the spray-pyrolysis process, PVSK precursors were dissolved in DMF and sprayed at the surface temperature of 75 °C. These substrates were then annealed under a hot-air assisted process to obtain highly crystalline and uniform PVSK thin films. The continuous heat flow provided a two dimensional, uniformly directional flow at the air–liquid interface to promote the crystallization of PVSK and remove the volatile byproducts. The distance between the heat gun (Pro-Heat 1100 Dualtemp, Master Appliance) and the substrate was kept at 21 cm to maintain a temperature of 110 °C at the substrate surface. The moving stage was iteratively oscillated at a speed of 5 mm s^{-1} during annealing to ensure uniformity. The annealed samples appeared to be dark brown in color, however at higher humidity the samples turned metallic grayish in color. Next, 2 wt% of C_{60}PCBM (Nano-C) dissolved in dichlorobenzene was spin-coated onto the as-prepared thin film at 3000 rpm and then annealed at 100 °C for an hour. Another 30 nm of C_{60} was thermally evaporated as an additional blocking layer. 70 nm of aluminum was then thermally evaporated to complete the devices. The photovoltaic performance was characterized by a Keithley 2400 source measurement unit under a simulated AM 1.5G spectrum. QE-5 measurement system (Enli Tech., Taiwan) was used to acquire the external quantum efficiency (EQE) spectra.

Characterizations

The morphological and topological information of PVSK thin films were obtained using a combination of FESEM (Zeiss, ULTRA-55), atomic force microscopy (AFM, Multimode, DI), and optical microscopy (Leica, DM-2500). Thickness of PVSK thin films was determined through cross sectional SEM images. The X-ray diffraction (XRD) characterizations were collected using a Bruker AXS D8 Discover GADDS X-ray diffractometer (Cu Kα radiation, $\lambda = 1.54059$ angstrom). A pulsed supercontinuum source (NTK Photonics) at 690 nm wavelength with 1.2 mW cm^{-2} power density was used for optical measurements. The photoluminescence (PL) measurements were done using an Action 150i spectrometer, which disperses the signal onto a thermoelectrically cooled CCD. For time-resolved PL measurements, a 690 nm pulsed light source was used at a Rep rate of 3.9 MHz.

3. Results and discussions

Tears of wine, as shown in Fig. 1, occurs when two miscible solvents, in this case water and alcohol, have different vapor pressures. Upon drying, alcohol evaporates much faster than water, leaving behind a gradient in surface tension. Such a difference in localized surface tensions promotes capillary flows towards the evaporation sites[25] in order to reach a new

Fig. 1 Representative photograph shows the uniform coating of red wine at macroscale enabled by the Marangoni flow. The dissimilar evaporation rates between each solvent result in advancing solvent fronts toward un-wetted areas.

equilibrium. Specifically, such an interfacial surface tension gradient first and foremost retards the receding liquid on the glass wall and creates viscous flow to facilitate subsequent film spreading. As alcohol keeps evaporating in the open system, the upward force decreases with the amount of alcohol in the liquid film and finally the water droplets fall down and form traces of "tears" that give its special terminology. The competing and replenishing processes of two miscible solvents have been characterized as Marangoni flow, which describes the hydrodynamic interactions among liquid species with gradients in either temperature, surface tension, solute concentration, or vapor pressure.[20,22,26–28] The presence of such gradients will provide a driving force to facilitate the system to dynamically achieve a new equilibrium. When the driving force is continuous, as in the previous example, the microscopic mixings of two solvents inevitably create high frequencies of solute exchange and collision that ultimately prevent pinning of the droplets to the surface, resulting a uniformly distributed liquid thin film with seemingly infinite interfaces among spices. Previous studies have demonstrated that this natural phenomenon resulting in translucency of glass walls after swirling of two liquids with different vapor pressure can be successful transcribed to the rapid and high throughput production of a variety of polymeric nanomaterials, inorganic nanoparticles. The resulting thin films were found to possess morphological homogeneity with ordered packing at nanoscale. Of particular importance this film growing technique can be readily scale up and consume only a fractional amount of solutions compared to other casting techniques, such as spin-coating. We are thus interested in studying how the Marangoni effect regulates the hydrodynamics of PVSK containing droplets to create a uniform and pinhole-less thin film that is essential for efficient absorption and subsequent transportation of charge carriers in conjunction with efficient management of Pb consumption.

It is known that Marangoni effect is governed by complex and dynamic liquid–liquid and liquid solid interactions.[20,28] The equation can be expressed as

$$V_c^2(x) = \frac{1}{2\eta(x)} \frac{d\sigma}{dx} x(1-x)(-A_l\alpha_l + A_h\alpha_h),$$

where V_c is the Marangoni velocity, η is the viscosity of the film, σ is the surface tension, x is the volume fraction of the low surface tension solvent, and A is the evaporation capacity, induced by evaporation from a two-component mixture. We found that the difference between vapor pressures of solvent combinations has a significant effect on the aforementioned interactions. To maximize the wetting and subsequent spreading of thin film, we initially adopted the solvent combination of DMF (surface tension, 37.1 mN m^{-1} at 20 °C) and DMSO (43.54 mN m^{-1} at 20 °C). PVSK precursors solution comprising MAI, and $PbCl_2$ (molar ratio, 3 : 1; 2.64 M for MAI, and 0.88 M for $PbCl_2$) is first dissolved in a mixture of anhydrous DMSO, and DMF (1 : 1, v/v) and fed through an EHD deposition, also known as electrospray, as schematically illustrated in Fig. 2a. Unlike those by spray-pyrolysis, incoming droplets are preferentially deposited onto the ITO substrate (1.4 cm by 1.6 cm) pre-coated with PEDOT:PSS (40 nm) in the presence of electric fields, thus enhancing the coverage and fidelity.[29] Unfortunately, we found that most of incoming droplets immediately pinned on the substrate and dried without coalescing. As shown in Fig. S1a,† the film displayed a crater-like morphology and was found to fill with pores in between discontinuous islands when characterized under an optical microscope. SEM together with AFM shows that the number of pores decreases, but their size increases as PVSK precursors crystallized to reach a low energy state upon annealing at 110 °C for 7 minutes using a heat gun. Cross-sectional SEM further reveals that a thin film thickness of 600–650 nm. However, the cross-section is primarily made of small PVSK crystals packed in an irregular fashion. The dimension of crystals falls in the range of 100 to 200 nm as determined by SEM, representing unwanted recombination centers for charge carrier transport.

Even though previous strategies already reported that the use of DMSO forms the intermediate phases with self-organizing capabilities, the overall morphology is intriguingly consistent with the previous study when employing DMF only spray.[21,30] We thus suspect the volatile nature (low surface tension) of DMF is primarily accounted for the de-wetting of PVSK thin films. To understand the influence of surface tension variation on thin film morphology, we systematically vary the volume ratio of DMF in the binary solvent systems. Decreasing the volume ratio of volatile DMF results in marginally greater coverage as shown in Fig. S1b.† Although AFM and SEM images from the thin film with the highest coverage (70% from DMSO : DMF, 9 to 1, v/v) collectively indicate the growth of PVSK crystals (average 500 to 750 nm), it is the lack of secondary solvent that diminishes the Marangoni effect. Thus, the PVSK droplets will only undergoes coalescence without advancing toward un-wetted area, leaving behind pinholes or narrow slits between network-like PVSK crystals. On the other hand, granular cross-section begins to merge and form a single grain like pathway in a vertical direction. This unique structural feature can be particular advantageous in the case of planar heterojunction architecture as the photo-dissociated charge carriers can propagate without encountering grain boundaries, thus enhancing the collecting efficiency at both electrodes. If we can suppress the unwanted de-wetting process stemmed from both the pinning and stagnant solvent fronts (Fig. S1c†), PVSK thin film with an improved coverage and preserved crystallinity in both in-plane and out-of-plane directions can be obtained. This will in turn synergistically increase the absorption, and transportation of PVSK thin films, ultimately giving rise to competitive PCE.

With this concept in mind, an ideal solvent should be less volatile and miscible with DMSO while possessing similar surface tensions with DMF. Indeed, when replacing DMF with *N*-methyl-2-pyrrolidione (NMP, 40.79 mN m^{-1} at 20 °C) and carefully controlling the volume ratio (DMSO : NMP 4 to 6, v/v), PVSK droplets immediately coalesce and merge into a yellow translucent film with a full coverage as shown in Fig. 2b. Specifically, the PVSK thin film remains wet even placing inside the glove box for 30 minutes by virtue of the formation of DMSO-legated intermediate phases (stage I and Fig. S2†). Such

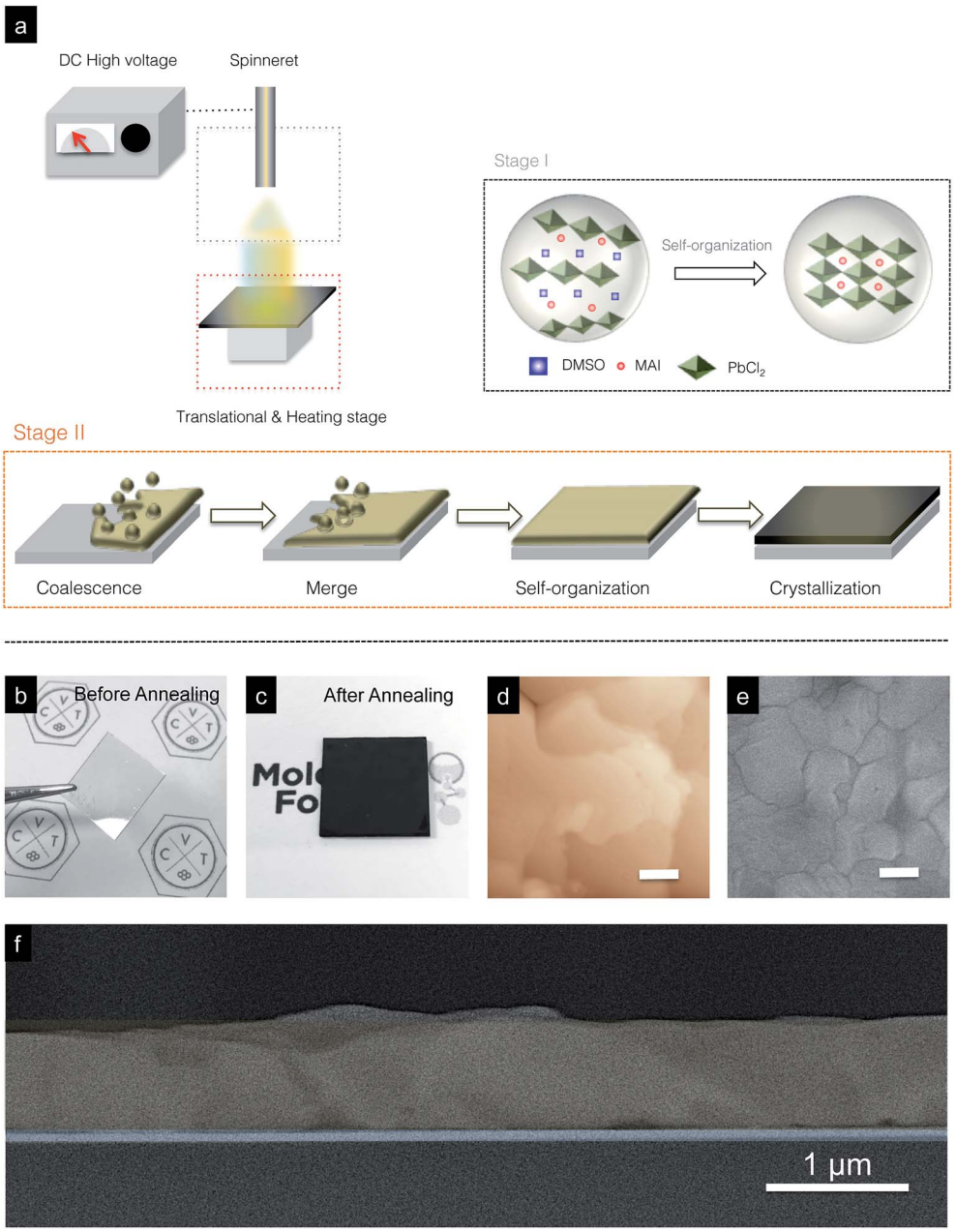

Fig. 2 (a) Schematic illustration shows the EHD setup that enables self-organization (stage I) and optimization of hydrodynamics of PVSK containing droplets (stage II). Photographs of PVSK thin films (b) before and (c) after annealing suggest the uniform coverage throughout the entire ITO substrate. (d) AFM and (e) HRSEM characterizations further confirm the advantageous topology and morphology in conjunction with a slab like cross-section (f). Scale bars are 200 nm and 2 μm, respectively.

an intermediated phase is known to enable self-organization of PVSK precursors into ordered structures, thus forming a solid foundation for subsequent annealing process. In addition, the marginal differences of surface tensions can already initiate the initially stationary solvent fronts without inducing the de-wetting of thin films upon transforming into highly crystallized PVSK (stage II, and Fig. 2c). The resulting thin films exhibit a dark, brownish color as well as a significantly higher absorbance across the entire the visible range, an indication of high coverage (Fig. S3a†). Photoluminescence (PL) measurement also showed a broad Gaussian spectrum with a characteristic center wavelength of 775 nm, while the presence of sharp (110) and (220) peaks in XRD data confirm the full conversion into highly crystallized PVSK (Fig. S3a in blue and S2† in red).[2,23,31–35] As shown in morphological and topological characterizations (Fig. 2d and e), the coalescing and merging of droplets in conjunction with the propagating solvent fronts result in an extremely smooth thin film with reduced surface roughness (~8 nm). The Marangoni effect also enables a dynamic growing process of the PVSK crystals as the average in-plane grain size

(~5 μm) well exceeds the thickness of thin films in a way similar to the solvent annealing process although with a much shorter processing time. In particular, the cross-sectional SEM image reveals sharp, continuous and slab-like grains without obvious grain boundaries as suggested in Fig. 2f. Further, cross-sectional SEM along with EDX mapping collectively confirm the spatial distribution of relevant elements, such as Pb in yellow, I in cyan and Cl in red (Fig. S4†). The synergistic growth of grains in all directions can be translated into the establishment of energetically favorable pathways without the presence of recombination centers. Meanwhile the versatility of the Marangoni-assisted deposition is further demonstrated through achieving a uniform deposition on a 15 mm by 50 mm ITO substrate; flexible ITO and fluorine doped tin oxide (FTO) with high coverage and low surface roughness as shown in Fig. S5.†

We also analyzed the temperature dependent morphology evolution on the final solid film of PVSK. At a low substrate temperature (30 °C) during deposition, the hydrodynamics of incoming droplets show a complete wetting of the whole surface (Fig. 3a). With a drying time ≥30 minutes, the PVSK droplets completely settle into uniform films without contracting. The film showed high uniformity and coverage (~95%, characterized by image-J) before and after annealing with some mild rippling scattering around the edges. The coverage significantly reduced when deposition was carried out at a substrate temperature of 50 °C. Upon deposition, PVSK droplets initially begin to settle into full film along the center of the deposition. Dynamic spreading was observed under a high-speed camera, but is soon stopped by contraction that prevents the full converge. Instead, the drying time of PVSK thin film drastically reduces to 30 seconds. The fast evaporation rate also in turn induces the reduction of grain size (~500 nm). The resulting film reveals the combination of pinholes and coffee ring like drying patterns that deteriorate the overall uniformity under optical microscopy (Fig. 3b). Although the coverage still remains around 85%, the presence of irregular undulations brought the surface roughness up to few hundred nm. When the annealing temperature further elevates to 70 °C, most of the liquid droplets immediately dried upon deposition with only few sessile droplets leave on the ITO substrate. Upon annealing, the resulting film was found to develop a streak-like morphology with the overall coverage fell behind 40% as shown in Fig. 3c. Specifically, the enhanced evaporation rate in the close proximity of droplet contact lines creates inward fluxes, thus leading the accumulation of solute along the perimeter of the deposition. Thus, the flash drying behavior results in the formation of large clusters interspersed in between small, irregular shaped islands of PVSK grains. These experimental observations also mesh well with spectral PL characterization results. The PL peak centered at 775 nm featured in Fig. 3d is used as the index to measure the uniformity across a rectangular region of 50 μm × 15 μm with a step size of 5 μm. As expected, the spatially-resolved PL mapping appeared to be more uniform when surface temperature is set at 30 °C (upper panel, Fig. 3e), whereas many dark regions arise when surface temperature increases to 50 °C as shown in the middle panel. At 70 °C, the majority of the PL mapping turns into a dark brown or black color, suggesting the clustering or aggregation of grains into discrete islands as a result of de-wetting process (bottom panel). Since high coverage with uniformity is the prerequisite for efficient solar-to-electricity conversion, knowing these parameters will help us formulate a robust protocol in fabrication of PVSK photovoltaics with a high yield of reproducibility and fidelity. Complete parameters of EHD deposition and the associated morphology can be found in Table 1.

Aside from the improved coverage and preserved crystallinity, the PVSK films made by Marangoni assisted deposition also display an average lifetime of ~180 ns when measured under time-resolved photoluminescence lifetime (TRPL) measurement (Fig. S4b†). Specifically, the lifetime can be deconvoluted into a bimodal recombination process that is commonly observed in the PVSK specimens with large, continuous grains, consistent with the previous reports.[11,21] From a photovoltaic perspective, the long lifetime can be translated to equivalently long carrier diffusion length within the bulk PVSK. The detailed device fabrication procedure is included in the methods section. Fig. 4a schematically depicts a complete planar device that comprises ITO/PEDOT:PSS/PVSK/C_{60}PCBM/C_{60}/Al along with the corresponding false colored, cross-sectional SEM image. Continuous and well-defined interfaces between PVSK and neighboring extraction layers can be clearly identified. In particular, the in-plane grain readily established transport pathways for self-dissociated charge carriers to propagate without trapping in between grain boundaries. Indeed, the average current–voltage (*I–V*) output characteristics from 28 devices collectively deliver an averaged short circuit current (J_{sc}) of 21.50 mA cm^{-2}, an open circuit voltage (V_{oc}) of 0.92 V, and fill factor (FF) of 72%, and a PCE of 14.24% under AM 1.5G (blue curve in Fig. 4b). Fig. S6a† shows the histogram of the distribution with regards to PCEs, with the highest PCE readily exceeding 16%. Note that the average PCE reported here already represents greater than a 1.5 times improvement over the PVSK photovoltaics prepared from conventional spray-pyrolysis approach (8.60%, orange curve in Fig. 4b). Further, thin film prepared from Marangoni assisted deposition only exhibit a minor hysteresis when scanned in both forward and reverse directions, possibly arising from the grain boundaries in contact with the neighboring transporting layers (affecting FF, Fig. S6b†). Meanwhile, EQE spectrum also follows the same increasing trend when employing Marangoni assisted deposition as shown in Fig. 4c. The EQE increases abruptly at the onset of characteristic bandgap at 790 nm and reaches a plateau around 600 nm. In particular, the average EQE in the visible range exceeds 80% while the PVSK prepared from conventional spray coating reaches 60%. Detailed *I–V* characteristics can be found in Table 2.

The substantial, near two-fold improvements on PVSK photovoltaics deposited by Marangoni-assisted process are due to the improved coverage and grain sizes: the significantly higher coverage has enabled collection of a higher fraction of incident photons at the same thickness, thus increasing the J_{sc} while the increase in grain size at all directions reduces both shunting pathways and defect/recombination sites would therefore be expected to enhance the FF and V_{oc} as we report

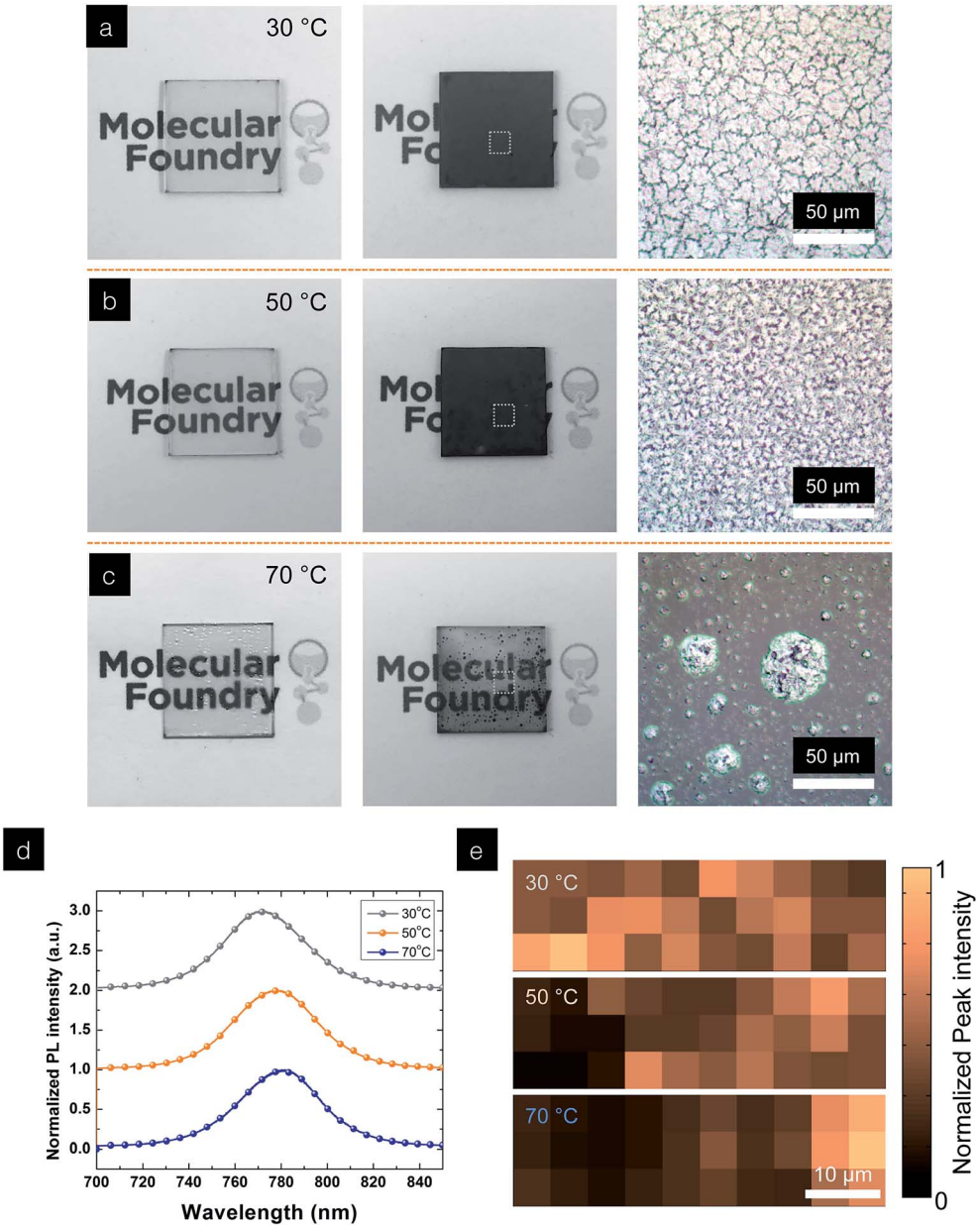

Fig. 3 Photographs along with optical microscopy images of PVSK thin films (645 mg mL^{-1} in 4 : 6 v/v, and 3.2 mm min^{-1}) deposited at various temperatures, (a) 30 °C, (b) 50 °C, and (c) 70 °C, respectively. (d) PL spectrum and (e) mapping across a 50 µm by 15 µm area collectively reveal the uniformity of PVSK crystals in the in-plane direction when the surrounding temperature is controlled at 30 °C. Meanwhile, rupture of thin films occurs immediately when annealing temperature rises to 70 °C, leading to the formation of jagged terrains and pinholes (dark regions).

here. Such trends are demonstrated in Fig. S7,† V_{oc} and J_{sc} show clear trends with coverage. Solvent ratios that reached the highest coverage in each case were selected for comparison. In particular, at coverage of 62% (DMF only case), average J_{sc} is around 14.5 mA cm^{-2}. Although the replacement of DMF by the binary solvent system (DMSO : NMP, 9 : 1) did improve the

Table 1 Complete parameters of the Marangoni-assisted EHD depositions and the resulting morphology deposited at a substrate temperature of 35 °C

Solvent	MAI : $PbCl_2$ 3:1 ratio (M)	Electric field (kV cm^{-1})	Flow (µL min^{-1})	Self-reorganization	Annealing (°C, min)	Morphology
DMF	2.64 : 0.88	5 kV cm^{-1}	18	15 min	110 °C for 7 min	Granular
DMSO : DMF 1 : 1	2.64 : 0.88	5 kV cm^{-1}	18	15 min	110 °C for 7 min	Discontinuous island
DMSO : DMF 9 : 1	2.64 : 0.88	5 kV cm^{-1}	18	15 min	110 °C for 7 min	Ragged terrain
DMSO : NMP 4 : 6	2.64 : 0.88	5 kV cm^{-1}	18	15 min	110 °C for 7 min	Continuous and uniform

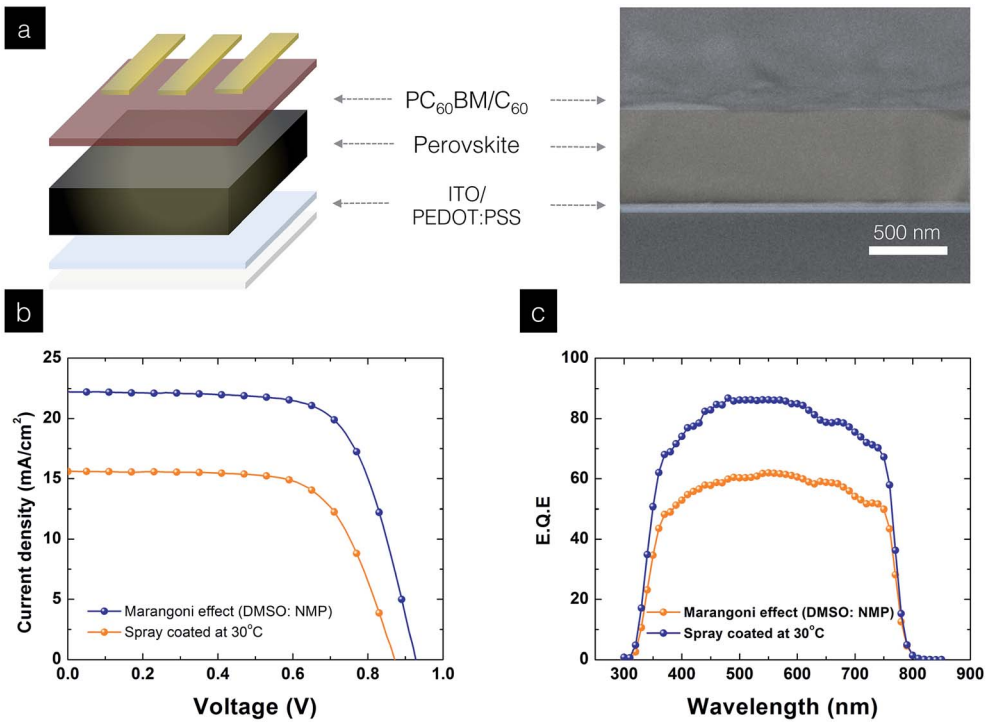

Fig. 4 (a) Schematic depicts the planar architecture of PVSK photovoltaics that consist of ITO/PEDOT:PSS/perovskite/C_{60}PCBM/C_{60}/Al. The corresponding cross-sectional HRSEM image shows the well-defined, continuous interfaces with the neighboring transport layers. (b) Average *I–V* curves (26 devices) measured from both Marangoni and conventional spray coating processes with 10 mV voltage steps, and 40 ms delay times under an AM 1.5G illumination. (c) Corresponding EQE also shows a substantial increase compared to that of spray-coated system.

Table 2 *I–V* output characteristics of DMF only and Marangoni-assisted process

Process	J_{sc} (mA cm^{-2})	V_{oc} (V)	FF (%)	PCE (%)
Spray-coated	15.4	0.86	65	8.6
Marangoni-assisted	21.5	0.92	72	14.2

effective coverage to 78%, it is the formation of pinholes that form the shunting pathway with neighboring layers. As a result, the overall photovoltaic characteristics are still far from ideal although the J_{sc} did increase due to the higher absorption (coverage). When the coverage increases up ~92% (Marangoni deposition from DMSO : NMP 4 : 6, v/v), J_{sc} increase linearly up to average values of 21.2 mA cm^{-2}, corroborate with our experimental observation that the higher coverage the better the absorption for generating available excitons. We thus can draw a logical conclusion that the use of Marangoni-assisted deposition enables the high coverage for associated absorption and carrier transportation, ultimately giving a boost to the PCE. In parallel, the ability to create uniform thin films with continuous grains in a single pass deposition also represents a very visible nexus between high throughput depositions and low material consumption, especially the perplexing Pb. To reach PVSK thin films with thicknesses of 600 nm on a 1.4 cm by 1.6 cm ITO substrate, it takes only 1.8 μL of the precursor solutions (2.64 M MAI : 0.88 M $PbCl_2$). Further, around 88–90% of the PVSK precursor droplets were electrically guided to deposit on the targeted surface. This is in turn equal to the consumption of 0.32 mg Pb during each deposition. The prospect of effectively managing the material consumption during scalable production holds great promise toward the widespread deployment of PVSK solar cells to meet the formidable energy challenges.

4. Conclusion

In conclusion, we transcribe the prevailing Marangoni flow in nature into an efficient deposition technique for the fabrication of highly uniform PVSK thin films with enhanced coverage and grain size. By the virtue of Marangoni flow which originated from the vapor pressure gradient in a binary solvent system, the PVSK precursor-containing droplets undergo a serial process of coalescence, merging and spreading that leads to a continuous thin film morphology without the needs for post-deposition engineering. Specifically, the use of less volatile NMP solvent suppresses the detrimental rupture of wet film upon annealing while enabling the dynamic grain growth of PVSK. These advantageous features collectively drive the average PCE to 14.2%, representing 1.5 times higher than that of conventional spray-pyrolysis process. Given the relatively simple device architecture, we envision that the PCE can be further improved through the use of more efficient charge extraction layers. Meanwhile, Marangoni-assisted deposition demonstrated here alleviates the impacts of excessive consumption of Pb during fabrication through effective management. With the rapid

advancement in compositional engineering and morphological tailoring, highly efficient PVSK photovoltaics with limited environmental impact can be envisioned through this massively parallel nanomanufacturing route.

Acknowledgements

V. T. gratefully acknowledge the support of user proposals (#3192 and #3715) at the Molecular Foundry, Lawrence Berkeley National Lab, supported by the Office of Basic Energy Sciences, of the U.S. Department of Energy under Contract No. DE-AC02-05CH11231 and NASA MIRO Center under Contract No. NNX15AQ01A. S. G. would like to acknowledge the National Science Foundation DMR-1056860. The authors are indebted to Daniel Sun, and Wendy L. Queen for XRD characterizations, Dr Yi Liu, Teresa L. Chen and Bradley Frank for the fruitful discussion in charge carrier dynamics and Marisol Prado for the assistance in instrumentation.

References

1 K. Liang, D. B. Mitzi and M. T. Prikas, *Chem. Mater.*, 1998, **10**, 403–411.
2 H. Zhou, Q. Chen, G. Li, S. Luo, T.-b. Song, H.-S. Duan, Z. Hong, J. You, Y. Liu and Y. Yang, *Science*, 2014, **345**, 542–546.
3 S. Sun, T. Salim, N. Mathews, M. Duchamp, C. Boothroyd, G. Xing, T. C. Sum and Y. M. Lam, *Energy Environ. Sci.*, 2014, **7**, 399–407.
4 Q. Chen, H. Zhou, Z. Hong, S. Luo, H.-S. Duan, H.-H. Wang, Y. Liu, G. Li and Y. Yang, *J. Am. Chem. Soc.*, 2014, **136**, 622–625.
5 D. W. de Quilettes, S. M. Vorpahl, S. D. Stranks, H. Nagaoka, G. E. Eperon, M. E. Ziffer, H. J. Snaith and D. S. Ginger, *Science*, 2015, **348**, 683–686.
6 M. M. Lee, J. Teuscher, T. Miyasaka, T. N. Murakami and H. J. Snaith, *Science*, 2012, **338**, 643–647.
7 H.-S. Kim, I. Mora-Sero, V. Gonzalez-Pedro, F. Fabregat-Santiago, E. J. Juarez-Perez, N.-G. Park and J. Bisquert, *Nat. Commun.*, 2013, **4**, 2242.
8 N.-G. Park, *J. Phys. Chem. Lett.*, 2013, **4**, 2423–2429.
9 N. J. Jeon, J. H. Noh, W. S. Yang, Y. C. Kim, S. Ryu, J. Seo and S. I. Seok, *Nature*, 2015, **517**, 476–480.
10 M. D. McGehee, *Nat. Mater.*, 2014, **13**, 845–846.
11 W. Nie, H. Tsai, R. Asadpour, J.-C. Blancon, A. J. Neukirch, G. Gupta, J. J. Crochet, M. Chhowalla, S. Tretiak, M. A. Alam, H.-L. Wang and A. D. Mohite, *Science*, 2015, **347**, 522–525.
12 Q. Wang, Y. Shao, Q. Dong, Z. Xiao, Y. Yuan and J. Huang, *Energy Environ. Sci.*, 2014, **7**, 2359–2365.
13 N. J. Jeon, J. H. Noh, Y. C. Kim, W. S. Yang, S. Ryu and S. I. Seok, *Nat. Mater.*, 2014, **13**, 897–903.
14 A. Dualeh, N. Tétreault, T. Moehl, P. Gao, M. K. Nazeeruddin and M. Grätzel, *Adv. Funct. Mater.*, 2014, **24**, 3250–3258.
15 J. Burschka, N. Pellet, S.-J. Moon, R. Humphry-Baker, P. Gao, M. K. Nazeeruddin and M. Gratzel, *Nature*, 2013, **499**, 316–319.
16 C. Bi, Q. Wang, Y. Shao, Y. Yuan, Z. Xiao and J. Huang, *Nat. Commun.*, 2015, **6**, 7747.
17 Q. Chen, H. Zhou, Y. Fang, A. Z. Stieg, T.-B. Song, H.-H. Wang, X. Xu, Y. Liu, S. Lu, J. You, P. Sun, J. McKay, M. S. Goorsky and Y. Yang, *Nat. Commun.*, 2015, **6**, 7269.
18 Y. Tidhar, E. Edri, H. Weissman, D. Zohar, G. Hodes, D. Cahen, B. Rybtchinski and S. Kirmayer, *J. Am. Chem. Soc.*, 2014, **136**, 13249–13256.
19 S. T. Williams, F. Zuo, C.-C. Chueh, C.-Y. Liao, P.-W. Liang and A. K. Y. Jen, *ACS Nano*, 2014, **8**, 10640–10654.
20 C. Girotto, D. Moia, B. P. Rand and P. Heremans, *Adv. Funct. Mater.*, 2011, **21**, 64–72.
21 A. T. Barrows, A. J. Pearson, C. K. Kwak, A. D. F. Dunbar, A. R. Buckley and D. G. Lidzey, *Energy Environ. Sci.*, 2014, **7**, 2944–2950.
22 R. D. Deegan, O. Bakajin, T. F. Dupont, G. Huber, S. R. Nagel and T. A. Witten, *Nature*, 1997, **389**, 827–829.
23 Z. Xiao, Q. Dong, C. Bi, Y. Shao, Y. Yuan and J. Huang, *Adv. Mater.*, 2014, **26**, 6503–6509.
24 J.-H. Im, I.-H. Jang, N. Pellet, M. Grätzel and N.-G. Park, *Nat. Nanotechnol.*, 2014, **9**, 927–932.
25 M. K. Chaudhury and G. M. Whitesides, *Science*, 1992, **256**, 1539–1541.
26 R. Vuilleumier, V. Ego, L. Neltner and A. M. Cazabat, *Langmuir*, 1995, **11**, 4117–4121.
27 Y. Cai and B.-m. Zhang Newby, *J. Am. Chem. Soc.*, 2008, **130**, 6076–6077.
28 X. Fanton and A. M. Cazabat, *Langmuir*, 1998, **14**, 2554–2561.
29 A. Jaworek and A. T. Sobczyk, *J. Electrost.*, 2008, **66**, 197–219.
30 M. Ramesh, K. M. Boopathi, T.-Y. Huang, Y.-C. Huang, C.-S. Tsao and C.-W. Chu, *ACS Appl. Mater. Interfaces*, 2015, **7**, 2359–2366.
31 M. Liu, M. B. Johnston and H. J. Snaith, *Nature*, 2013, **501**, 395–398.
32 Y. Wu, A. Islam, X. Yang, C. Qin, J. Liu, K. Zhang, W. Peng and L. Han, *Energy Environ. Sci.*, 2014, **7**, 2934–2938.
33 Z. Yang, C.-C. Chueh, F. Zuo, J. H. Kim, P.-W. Liang and A. K. Y. Jen, *Adv. Energy Mater.*, 2015, **5**, 1500328.
34 H. Yu, F. Wang, F. Xie, W. Li, J. Chen and N. Zhao, *Adv. Funct. Mater.*, 2014, **24**, 7102–7108.
35 W. Zhang, M. Saliba, D. T. Moore, S. K. Pathak, M. T. Hörantner, T. Stergiopoulos, S. D. Stranks, G. E. Eperon, J. A. Alexander-Webber, A. Abate, A. Sadhanala, S. Yao, Y. Chen, R. H. Friend, L. A. Estroff, U. Wiesner and H. J. Snaith, *Nat. Commun.*, 2015, **6**, 6142.